JACS
JOURNAL OF THE AMERICAN CHEMICAL SOCIETY

ARTICLE

pubs.acs.org/JACS

Isolated Monohydrates of a Model Peptide Chain: Effect of a First Water Molecule on the Secondary Structure of a Capped Phenylalanine

Himansu S. Biswal, Yohan Loquais, Benjamin Tardivel, Eric Gloaguen,* and Michel Mons

Laboratoire Francis Perrin, CEA/DSM/IRAMIS/SPAM—CNRS URA 2453, CEA/Saclay, 91191 Gif-sur-Yvette, France

Supporting Information

ABSTRACT: The formation of monohydrates of capped phenylalanine model peptides, CH_3-CO-Phe-NH_2 and CH_3-CO-Phe-NH-CH_3, in a supersonic expansion has been investigated using laser spectroscopy and quantum chemistry methods. Conformational distributions of the monohydrates have been revealed by IR/UV double-resonance spectroscopy and their structures assigned by comparison with DFT-D calculations. A careful analysis of the final hydrate distribution together with a detailed theoretical investigation of the potential energy surface of the monohydrates demonstrates that solvation occurs from the conformational distribution of the isolated peptide monomers. The distribution of the monohydrates appears to be strongly dependent on both the initial monomer conformation (extended or folded backbone) and the solvation site initially occupied by the water molecule. The solvation processes taking place during the cooling can be categorized as follows: (a) solvation without significant structural changes of the peptide, (b) solvation inducing significant distortions of the backbone but retaining the secondary structure, and (c) solvation triggering backbone isomerizations, leading to a modification of the peptide secondary structure. It is observed that solvation by a single water molecule can fold a β-strand into a γ-turn structure (type c) or induce a significant opening of a γ-turn characterized by an elongated C_7 hydrogen bond (type b). These structural changes can be considered as a first step toward the polyproline II condensed-phase structure, illustrating the role played by the very first water molecule in the solvation process.

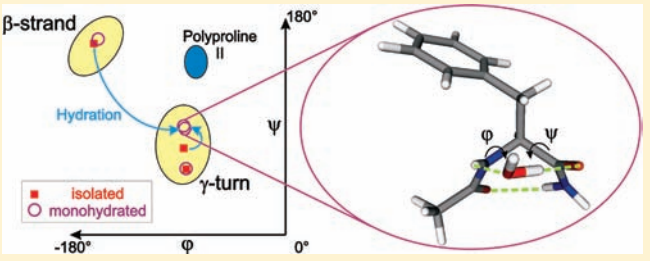

1. INTRODUCTION

Complete understanding of the link between the environment within which a protein resides and its secondary structure is still far from being achieved. From a theoretical point of view, modeling of a solvated protein chain as simple as the alanine dipeptide analogue (Ac-Ala-NH-Me) is still a subject of debate for molecular dynamics studies.[1,2] On such small systems, two-dimensional infrared spectroscopy (2D IR), nuclear magnetic resonance spectroscopy (NMR), vibrational Raman spectroscopy optical activity (VROA), or vibrational circular dichroism (VCD) of peptides in liquids can provide conformational characterization[3−7] as well as a few structural parameters that can be used for benchmarking purposes.[8,9] These approaches, however, suffer in general from an averaging over the whole distribution of conformers present in the medium. Alternatively, gas-phase spectroscopy experiments provide accurate and conformer-selective data but are limited to isolated systems. One approach to address solvation issues and still benefit from the spectral resolution of gas-phase measurements consists of studying mixed solvent/solute molecular clusters, where the number of solvent molecules in the system can be controlled.[10] Such microsolvated solutes (typically with less than 10 solvent molecules) are intermediate systems which can bridge the gap between isolated and fully solvated molecules, as they provide a unique insight into the solvation process by eventually revealing the role of every single solvent molecule. The effect of a modest number of molecules, which was already suspected from basic *ab initio* calculations,[9] can now be addressed experimentally for a large panel of systems using state-of-the-art spectroscopy coupled to efficient vaporization techniques.[11−13] Infrared/ultraviolet (IR/UV) double-resonance spectroscopy is a popular method which provides single-conformer IR spectra and is thus adapted to flexible systems like peptides. Coupled with the powerful computational arsenal of quantum chemistry, the data provided enable spectroscopists to characterize the conformations adopted by the peptides in the gas phase.[13−15] This approach has proven to be a unique tool in revealing the underlying noncovalent interactions like H-bonds, NH-π bonds, or aromatic−aromatic interactions that control the conformational preferences adopted by short peptides.[16−18]

In this context, gas-phase solvation studies appear quite promising for a complete characterization of microsolvated structures, thus providing a better understanding of solvation processes. Examples can be found in the literature on flexible molecules like tryptamine or 3-indolepropionic acid,[19,20] in which a water bridge is found to modify the conformational

Received: September 24, 2010
Published: February 28, 2011

dx.doi.org/10.1021/ja108643p | J. Am. Chem. Soc. 2011, 133, 3931–3942

preferences: solvation triggers a conformational isomerization, giving rise to the formation of unseen conformers in the isolated molecule. Laser-controlled isomerization between both hydration sites of a peptide bond has also been investigated on a rigid model molecule.[21] Spectroscopic studies dedicated to solvated peptides, however, remain sparse, primarily because their vaporization requires either a heating of the sample, which can cause pyrolysis, or laser evaporation sources, which remain difficult to handle and optimize for cluster formation. In addition, the size of these systems also makes spectroscopic investigations challenging. In IR spectra, it is difficult to disentangle reliably the NH and OH contributions because of the poor theoretical description of these vibrations.[22] In microwave experiments, the system size is limited by the spectral range of standard spectrometers.[23,24]

A few microsolvated amino acids or peptide-like molecules, however, have been experimentally studied recently.[7,23,25−28] Combined experimental and theoretical analysis of these results revealed the effects of microsolvation on the molecular structure. Single hydration of natural amino acids, phenylalanine (H-Phe-OH) or glycine (H-Gly-OH), causes little change to the isolated amino acid structure.[23,25] Microhydration of a capped phenylalanine model molecule (Ac-Phe-O-Me) induces only slight backbone distortions up to two water molecules.[28] In this case, three water molecules were needed to affect significantly the backbone arrangement. Microsolvation has also been observed to potentially induce changes in the conformational distribution,[25−27] as already reported for tryptamine.[19,20,29,30] Conformational preferences can also be dramatically inverted between isolated and microsolvated species, as observed on melatonin[31] or on sugars.[32] It should nevertheless be noticed that in natural amino acids or in the capped peptide Ac-Phe-O-Me, the biologically relevant -CONH- peptide units are incomplete. As some of the H-bond donors and acceptors sites are missing, this too simple description prevents these systems from being suitable models for peptide chains. Only very recently, Zhu and co-workers[27] showed on a capped dipeptide that the preferred conformation switched from a γ-turn to a β-turn when only two methanol molecules were added to the isolated peptide.

The capped amino acids Ac-Gly-NH-Me and Ac-Ala-NH-Me are the simplest systems relevant to investigate the hydration of a peptide backbone; however, they have not yet been reported in the gas phase, despite their importance in terms of benchmarking for comparison with theoretical models. At present, only matrix isolation spectroscopy has provided structural data about these capped amino acids.[7] Unfortunately, these systems are inaccessible to standard laser double-resonance spectroscopy, owing to the lack of a near-UV chromophore which is required to benefit from the conformational selectivity of this technique. The capped phenylalanine, however, is fully compatible with these techniques and has been extensively studied.[33−35] In particular, *N*-acetyl-phenylalanine-amide[33] (NAPA) is a small capped peptide chain with an acetyl group protecting the N-terminal side and an amide group on the C-terminal side (Figure 1). Three donor sites (H1, H2, and H3) and two acceptors sites (O1, O2) for H-bonding are expected to be the preferred hydration sites of this molecule. The majority of the cold isolated NAPA molecules (~80%) have a β-strand structure[33] where the extended backbone is stabilized by a C_5 interaction between H1 and O2, and the rest of the molecules are folded into γ-turn structures with a C_7 H-bond between O1 and H2 (these structures are further detailed in Figure 8, below).

This paper documents the structural and conformational distribution changes of NAPA induced by microhydration in order to better understand the processes at play during the solvation of an isolated peptide chain. This system will then enable us to investigate the impact of the first solvent molecule on both extended and folded conformations, in terms of deformations and changes in conformational distribution. The results obtained on the microhydration of *N*-acetyl-phenylalanine-*N*-methyl-amide (NAPMA), a molecule only differing from NAPA by a substitution of H3 by a methyl group (Figure 1), will also be briefly presented and used to support the analysis conducted on the NAPA:water system. It is worth mentioning that the -NH-CH_3 C-terminal side of NAPMA makes this molecule an even more biologically relevant model of a peptide chain than NAPA. However, the NH_2 group of NAPA makes its IR spectral analysis much more informative[13] and justifies why this system has been preferred to be extensively studied. This paper is then organized as follows: after an overview of the experimental and theoretical techniques employed (section 2), the most relevant monohydrated structures of NAPA calculated at the B97-D level are presented (section 3), the UV and IR/UV spectroscopy of the 1:1 complexes is then analyzed (section 4), and the four conformers observed are assigned by comparison of the experimental and calculated OH and NH stretch frequencies (section 5). The microsolvated structures are then compared to the isolated peptide conformers (section 6.1), and a microsolvation scheme accounting for the conformational distribution observed is proposed (section 6.2). Different kinds of conformer-dependent microhydration are reported and have been tentatively classified according to the deformation induced on the peptide structure.

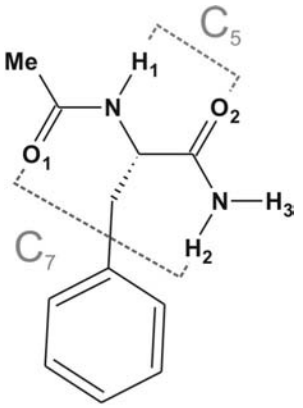

Figure 1. *N*-Acetyl-phenylalanine-amide (NAPA) molecule. Oxygen and hydrogen atoms that could possibly be involved in H-bonds are labeled along the backbone from the N-terminal to the C-terminal ends of the chain. The typical intramolecular interactions responsible for the extended (β-strand, with a C_5 H-bond) and folded (γ-turn, with a C_7 H-bond) backbone conformations are also presented. The *N*-acetyl-phenylalanine-*N*-methyl-amide (NAPMA) molecule is obtained by substituting the H3 atom by a methyl group.

2. METHODS

The NAPA:water complexes are formed by desorbing a 10:4:1 molar mixture of water, graphite, and NAPA, respectively, in a 10 Hz pulsed supersonic expansion of 6 bar of argon using the 532 nm light from a Nd:YAG laser. The complete design of this source has already been described elsewhere.[36] The molecular beam is skimmed before entering the interaction region of a time-of-flight mass spectrometer, where molecules and complexes are analyzed by IR/UV double-resonance spectroscopy.[16] UV light pulses of typically 400 μJ are produced by a BBO-doubled dye laser pumped

by an XeCl* excimer laser. Resonant two-photon ionization (R2PI) occurs when UV photons of appropriate wavelength excite the $\pi^* \leftarrow \pi$ transition of the phenyl ring, and UV spectra are obtained by recording the ion signal intensity as a function of the UV wavelength. The idler of a Nd:YAG-pumped optical parametric oscillator (OPO) source delivers IR light pulses of typically 1 mJ. Both $LiNbO_3$ and KTP crystals have been used to scan the 2.7−3.2 μm range covering the entire NH and OH stretch domains. Conformer-selective IR spectroscopy at a resolution of ~1 cm^{-1} is then performed by scanning the IR wavelength at fixed UV wavelength using the double-resonance IR/UV technique.[18,37]

Conformational explorations have been performed using the AMBER 99[38] and CHARMM 27[39] force fields included in the HyperChem Professional 7.51 package.[40] Several conformations were selected from these explorations for their potential ability to match the experimental IR spectra and were then optimized at the RI-B97-D/TZVPP level[41,42] employing the TURBOMOLE 5.10 package.[43] These calculations have also been complemented by optimizations of a few structures designed to explore more water and phenyl side-chain orientations than provided by the initial conformational explorations. The DFT-D method chosen was specifically designed to account for van der Waals interactions in large systems and has proven to provide accurate structures and energies, at least comparable to CCSD(T) results on benchmark systems.[44] Harmonic frequency calculations have been carried out at the same level of calculation, and mode-dependent scaling factors (Supporting Information (SI), Appendix S1) have been applied for comparison to the experimentally observed IR frequencies for conformational assignment purposes. The ability of mode-dependent scaling factors to accurately predict IR frequencies has been discussed in recent papers.[16,45] In the present case of peptide chains, the correlation between the experimental spectra collected in the past 5 years and the calculated harmonic vibrational frequencies (SI) has led us to apply linear mode-specific corrections to the calculated frequencies. The agreement between theoretical and experimental frequencies expected after such a scaling procedure is typically of ±~20 cm^{-1}. Energies are presented without basis set superposition error (BSSE) correction unless stated.

3. THEORETICAL RESULTS

From the monohydrate conformations found in the explorations (section 2), 125 structures were selected according to their stability and their consistency with experimental data (section 4) and have thus been optimized at the RI-B97-D/TZVPP level. As some of them were identical after geometry optimization, only 69 different conformations have eventually been considered. Four structural parameters can be defined in order to label these conformations: the shape of the backbone, the orientation of the phenyl ring, the hydration site, and the orientation of the water molecule relative to the peptide backbone. Labels in italics are used for theoretical conformers in order to distinguish them from the experimental ones.

Most of the backbone shapes of this set of conformations can be classified in three main categories: extended (***E***), folded (***F***, with two subcategories F^L and F^D), and intermediate (***I***) structures (Figure 2). ***E*** and F^L backbones are β-strands and γ_L-turns stabilized by C_5 and C_7 interactions, respectively. These structures have already been experimentally characterized for the isolated NAPA system.[33] As the γ-turn is a chiral structure[18] which can be of L or D conformation, a distinction is thus made between F^L and F^D backbones. In the ***I*** backbones, the water molecule is part of the secondary structure of the peptide. This structural water leads to partially folded backbones which are intermediate between ***E*** and ***F*** forms and thus typical of micro-hydrated conformations. ***I*** is also a chiral structure, but only the enantiomer form shown in Figure 2 has been found. Other backbone structures (***P***) are also found as minima of higher energy in the hydrate but have never been observed as isolated monomers in any gas-phase experiments.

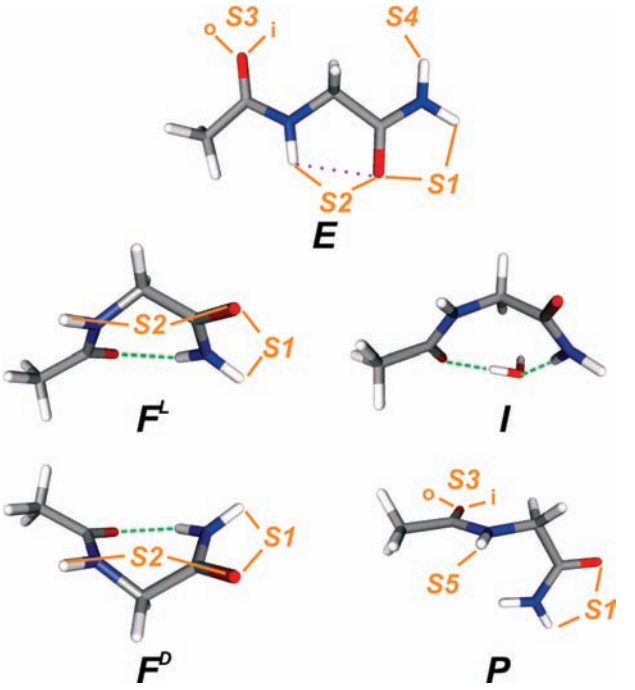

Figure 2. Different types of backbone arrangements (***E***, F^L, F^D, ***I***, and ***P***) and their main solvation sites (***S1***−***S5***) resulting from B97-D/TZVPP optimizations.

Phenyl side-chain orientations are labeled according to the value of the $NC^{\alpha}C^{\beta}C^{\gamma}$ dihedral angles gauche (***g***±) if the angle lies between 0 and ±120° and anti (***a***) otherwise.[33]

It is expected that the preferred solvation sites for the water molecules are those where at least one strong intermolecular H-bond is possible. These solvation sites have to be defined *a priori* for each peptide conformation. In order to facilitate comparison between conformations, however, we use the following labeling: ***S1*** when water bridges O2 and H3; this is the most commonly found solvation site, as the distance between O2 and H3 is fixed by the rigid peptide bond and thus does not depend on the conformation (Figure 2). Similarly, H1 and O2 define solvation site ***S2***, which is also a bridging site mostly found in ***E*** and ***F*** structures. The main remaining sites, ***S3***, ***S4***, and ***S5***, involve the O1, H2, and H1 atoms, respectively, in conformations with only one strong intermolecular H-bond. Finally, conformations with an ***I*** backbone do not need a solvation site to be specified, as water is always bridging O1 and H2 by definition.

Most of the solvation sites correspond to a set of multiple wells of the potential energy surface (PES) related to different orientations of the water molecule. In order to keep simple notations, a labeling is proposed, based on the orientation of the molecules shown in Figures 6−8, below: the phenyl ring lies above the backbone and the $C^{\beta}C^{\gamma}$ bond is oriented vertically, making the peptide bonds to lie roughly in a "horizontal" plane. The notation "up" (***u***) or "down" (***d***) then refers to the free OH group of water pointing either toward the phenyl direction or toward the opposite direction. In addition, both lone pairs of the O1 atom lead to multiple water orientations around solvation site ***S3***. Labels "in" (***i***) and "out" (***o***) are used to identify the lone pair interacting with water (Figure 2). Finally, when the oxygen atom

of water is significantly located out of the "horizontal" plane, the "vertical" site position of water is indicated by the label *v*.

Table 1 reports the energetics and scaled frequencies of the 39 most relevant conformations for assignment purposes from the set of the 69 calculated structures. This reduced set of conformations comprises all conformations ***I***, conformations ***E*** and $\boldsymbol{F^L}$ for which at least one strong intermolecular H-bond exists, and a selection of the most stable ***P*** and $\boldsymbol{F^D}$ conformations. It can be seen from this table that the conformational landscape of the NAPA:water system is made of several minima quite close in energy (most of these conformations are within a ∼15 kJ mol^{-1} energy range). However, the large frequency domains covered by the calculated frequencies (∼100 cm^{-1} for the NH_2^{anti}, ∼200 cm^{-1} for the NH_2^{sym} and NH stretches, and ∼300 cm^{-1} for the OH(1) stretch) suggest that these conformations can be accurately characterized and distinguished by their experimental IR fingerprint.

4. EXPERIMENTAL RESULTS

The R2PI signals of NAPA:water complexes are detected in the NAPA ion mass channel, leading to an overlap of the signatures of both NAPA:water and NAPA species on the UV spectrum (Figure 3). The main UV features due to complexes can be easily discriminated against the transitions of the isolated molecule by comparison with the spectrum of a pure NAPA/graphite tablet sample. IR spectra further confirm the assignment of these features to 1:1 complexes and not to fragmented larger clusters. The signal recorded on the NAPA:water ion mass channel allows us to estimate that at least ∼80% of the ionized complexes are fragmenting and that all major NAPA:water conformers are detected in the NAPA ion mass channel. Similar efficient fragmentation upon R2PI detection has been previously observed for the monohydrated phenylalanine[25] and other clusters.[46,47] Finally, one can notice that the conformational distribution of the isolated peptide does not show any measurable change when switching from dry to wet conditions, despite a significant decrease of the total ion signal of the monomer. One can deduce that water in the expansion does not significantly affect this conformational distribution and that water binds to the peptide with a weak conformer selectivity if any.

The IR spectra (Figure 4) reveal four different main conformers of the NAPA:water complex, labeled **W**, **X**, **Y**, and **Z**. For **W**, **Y**, and **Z**, five absorption bands corresponding to two OH, one NH, one NH_2^{sym}, and one NH_2^{anti} stretching modes are observed, as expected in this spectral region. One can notice that **W** has two bands well resolved at 3380 and 3388 cm^{-1}, the former being much weaker than the latter (Figure 4, inset). In contrast, **X** exhibits six bands. One could postulate **X** to be a 1:2 NAPA:water complex; however, seven bands would be expected in such a case. In addition, the band at 3565 cm^{-1} could not account for any kind of NH stretch: the upper value of ∼3550 cm^{-1} is reached for the NH_2^{anti} stretch of a free NH_2 group.[47] The band at 3565 cm^{-1} would then be assigned to an OH-bonded group, which is not consistent with its very low intensity.[48] One has to conclude that this weak band is likely to be a combination band and that the other five bands are the signature of the NH and OH stretches of a 1:1 NAPA:water complex. This conclusion is consistent with similar previous observations[26,49] and is supported by additional experiments carried out on the monohydrates of NAPMA. UV spectroscopy (SI, Figure S2) suggests that the conformers analogous to **W** and **X** also exist in NAPMA:water. The comparison between the IR spectra (Figure 5) clearly supports that $\mathbf{X}^{\mathbf{NAPMA}}$ has four bands, as expected for a monohydrate of NAPMA in this spectral region.

Table 1. Calculated Energetics and Scaled Harmonic Vibrational Frequencies of Selected NAPA:Water Conformations

	ΔG (kJ mol^{-1})[a]		vibrational frequency (cm^{-1})				
conformer	0 K	300 K	NH	NH_2^{sym}	NH_2^{anti}	OH(1)	OH(2)
E(a)S1u	5	4	3445	3347	3515	3451	3721
E(a)S1d	4	4	3446	3344	3513	3449	3720
E(a)S2u	7	6	3307	3416	3532	3467	3722
E(a)S2d	6	1	3305	3414	3531	3449	3719
E(a)S3id	3	4	3420	3414	3531	3417	3727
E(a)S3ou	11	7	3432	3419	3535	3458	3722
E(a)S3od	11	9	3430	3418	3534	3459	3722
E(a)S3v "Z"	**11**	**4**	**3430**	**3419**	**3535**	**3514**	**3724**
E(a)S4u	4	2	3441	3305	3508	3621	3726
E(g+)S1d	9	7	3449	3345	3532	3454	3719
E(g+)S2u	3	6	3267	3433	3550	3520	3676
E(g+)S2d	13	11	3312	3435	3553	3495	3717
E(g+)S3id	10	7	3429	3434	3551	3423	3725
E(g+)S3ou	17	13	3430	3436	3553	3459	3722
E(g+)S3v	14	11	3430	3439	3556	3482	3727
E(g+)S4u	17	14	3443	3383	3528	3653	3744
E(g−)S1d	15	12	3468	3341	3530	3446	3720
E(g−)S3v	15	16	3454	3430	3549	3525	3692
F^D*(g−)S1u*	9	10	3486	3314	3455	3416	3719
F^D*(g−)S2u*	9	11	3454	3329	3506	3472	3729
F^L*(a)S1u*	9	7	3467	3346	3488	3433	3718
F^L*(a)S1d*	9	7	3468	3350	3493	3433	3720
F^L*(a)S2u*	3	5	3351	3399	3520	3444	3725
F^L*(a)S2d*	3	5	3343	3403	3522	3425	3725
F^L(g+)S1u "Y"	**7**	**9**	**3442**	**3331**	**3464**	**3431**	**3718**
F^L(g+)S1d "Y"	**8**	**9**	**3442**	**3331**	**3465**	**3434**	**3719**
F^L*(g+)S2u*	3	8	3283	3384	3516	3574	3680
F^L*(g−)S1u*	7	6	3466	3331	3464	3428	3718
F^L*(g−)S1d*	8	7	3464	3332	3465	3428	3721
F^L(g−)S2u "X"	**2**	**3**	**3418**	**3381**	**3512**	**3446**	**3727**
F^L(g−)S2d "W"	**3**	**4**	**3376**	**3389**	**3516**	**3441**	**3725**
I(a)u	0*	1	3456	3280	3503	3385	3723
I(a)d	1	2	3458	3278	3503	3367	3726
I(g+)d	8	10	3448	3290	3494	3365	3726
I(g−)u	1	1	3466	3289	3501	3357	3726
I(g−)d	1	0*	3469	3271	3501	3343	3726
P(g+)S1u	10	8	3437	3352	3527	3433	3721
P(g+)S1d	8	7	3439	3351	3529	3425	3719
P(g+)S5u	5	8	3287	3412	3529	3614	3692

[a] Lowest energy conformations are marked with an asterisk (see section 3 for calculation details).

At this first stage of the NAPA spectroscopic analysis, it is already possible to propose an assignment for several IR features observed, based on general considerations about the IR spectroscopy (the larger the red-shift, the stronger the H-bond) as well as on previous experimental results,[13] in particular the correlation existing between symmetric and antisymmetric stretches of the NH_2 group of the C-terminal amide (Figure 5 of ref 13):

The free OH vibrational mode typically observed[48] at ∼3720 cm^{-1} is a common feature of the four conformers, indicating that water acts as a single H-bond donor in all four monohydrates.

No band is observed in the 3465−3495 cm^{-1} region, indicating that there is no free NH stretch[13] in these conformers.

The 3495−3550 cm^{-1} range is also very informative for assignment purposes, as it is accessible to the NH_2^{anti} stretch but not to the NH or NH_2^{sym} stretches. According to the correlation mentioned above,[13] the spectral position of the NH_2^{anti} stretch in this range provides a rough estimate of the corresponding NH_2^{sym} band position, which is indicative of the strength of the H-bond in which the NH_2 group is involved.

dx.doi.org/10.1021/ja108643p | J. Am. Chem. Soc. 2011, 133, 3931–3942

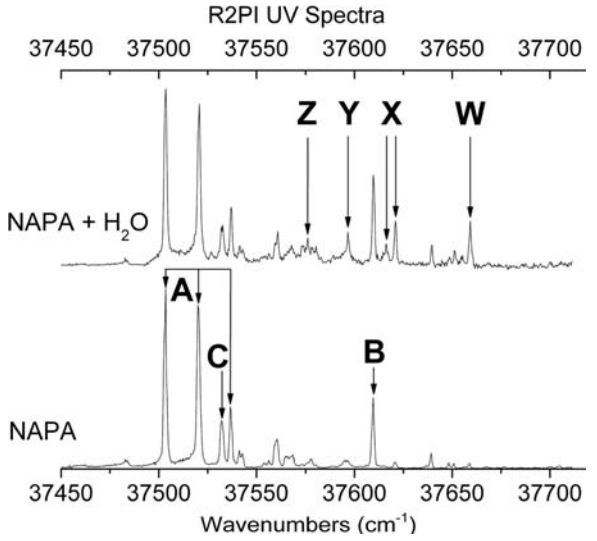

Figure 3. UV spectra recorded in the domain of the first $\pi^* \leftarrow \pi$ transition of the phenyl ring on the NAPA mass channel using dry (bottom) or wet (top) samples. **A**, **B**, and **C** are conformers of the isolated species previously assigned. The NAPA:water 1:1 complexs' main features are observed at 37 576, 37 597, 37 616, 37 620, and 37 659 cm^{-1}. Conformers of the monohydrated species are labeled **W**, **X**, **Y**, and **Z**.

The band of **W** at 3515 cm^{-1} can be assigned to the NH_2^{anti} stretch of a single H-bond donor NH_2 group. The same conclusion can be drawn for the band at 3510 cm^{-1} of conformer **X**. The correlations evoked above suggest that the corresponding NH_2^{sym} stretch should be found below ~3400 cm^{-1}. For **W**, it suggests that the NH_2^{sym} stretch is expected to be assigned to one of the components of the 3380/3388 cm^{-1} doublet. For **X**, the unique band measured in this region (3360 cm^{-1}) has thus to be assigned to the NH_2^{sym} stretch. This assignment is also supported by the comparison between the IR spectra of **X** and $\mathbf{X}^{NAPMA}$ (Figure 5): the common features at 3418 and 3446 cm^{-1} must be assigned to the NH1 and OH stretches, as the most red-shifted band must involve the different C-terminal sides of the two molecules. Such a comparison between **W** and $\mathbf{W}^{NAPMA}$ is unfortunately less fruitful, presumably due to vibrational couplings as mentioned earlier.

Conformer **Y** is the only one not to have a band in the 3495−3550 cm^{-1} range, indicating that the NH_2 group must be a double H-bond donor characterized by two red-shifted bands. As the NH group is also involved in a H-bond interaction, all three NH bonds of this conformer are H-bond donors, thus greatly reducing the number of structures capable of matching the IR spectrum. **Y** must then be assigned to a γ-turn (C_7 bond) structure (F^L or F^D) with a NH1$-\pi$ interaction and where the water molecule occupies site ***S1***.

Finally, conformer **Z** has the characteristic signature of a free or weakly bonded[13,33,47] NH_2 group, with two weak bands at 3440 and 3543 cm^{-1} corresponding to the NH_2^{sym} and NH_2^{anti} stretches, respectively. The alternative assignment for the NH_2^{anti} stretch to the band at 3507 cm^{-1} can be ruled out, as it would imply a large splitting of the NH_2 modes, leading to a NH_2^{sym} band well below 3350 cm^{-1} (Figure 5 of ref 13), whereas the lowest frequency band is actually observed at 3394 cm^{-1}. As the band at 3507 cm^{-1} is blue-shifted compared to the NH free stretch domain, it can only be assigned to an OH-bonded stretch mode, and finally the band at 3394 cm^{-1} can be assigned to the remaining NH stretch.

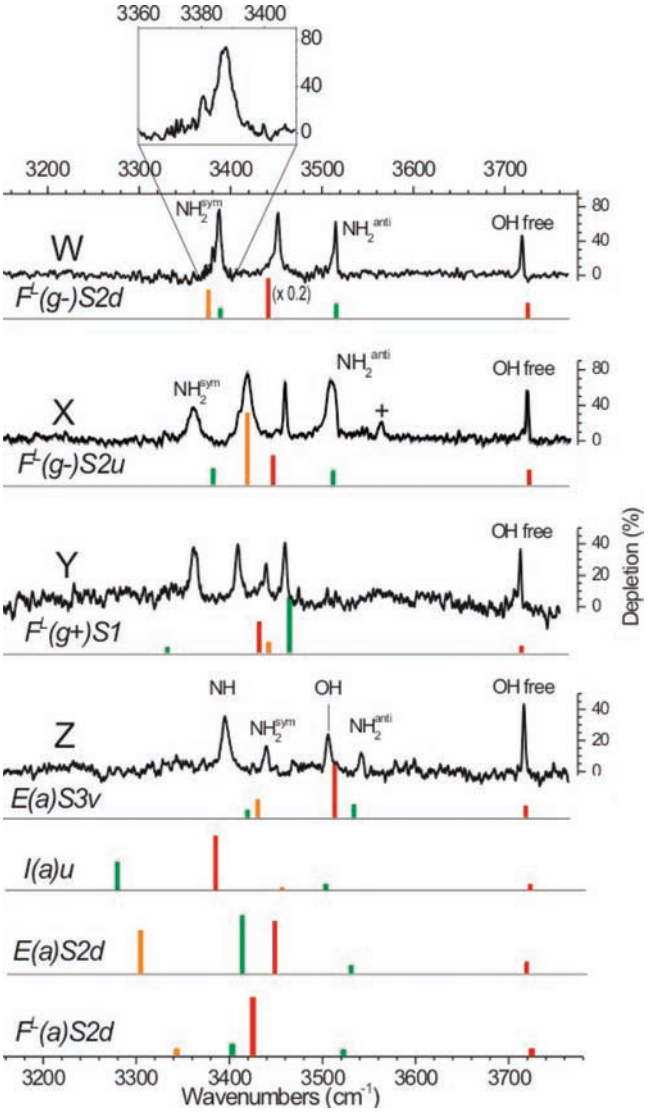

Figure 4. IR/UV double-resonance spectra of conformers **W**, **X**, **Y**, and **Z** recorded respectively at 37 659, 37 620, 37 597, and 37 576 cm^{-1}. Assignments are proposed for some of these bands from a spectral analysis detailed in the text. + marks a weak band due to a combination of vibrational modes. Bars represent the calculated frequencies and intensities of the OH (red), NH (orange), and NH_2 (green) stretching modes of the conformers relevant for discussion (Figures 6 and 7b, below).

These preliminary and partial mode assignments, deduced solely from a basic spectroscopic analysis, are summarized in the spectra of Figure 4.

5. CONFORMATIONAL ASSIGNMENT

Final assignment (Figure 4 and Table 2) has been achieved from the comparison between the experimental spectra and the set of harmonic frequencies from the 69 B97-D optimized structures as detailed in the next paragraph. Calculated intensities are also presented in Figure 4, although they are not reliable enough for assignment purposes owing to poorly predicted vibrational couplings (SI). The four calculated conformers $F^L(g-)S2d$, $F^L(g-)S2u$, $F^L(g+)S1u$, and $E(a)S3v$, finally assigned to the experimentally observed **W**, **X**, **Y**, and **Z** complexes, are shown in Figure 6.

dx.doi.org/10.1021/ja108643p | *J. Am. Chem. Soc.* 2011, 133, 3931–3942

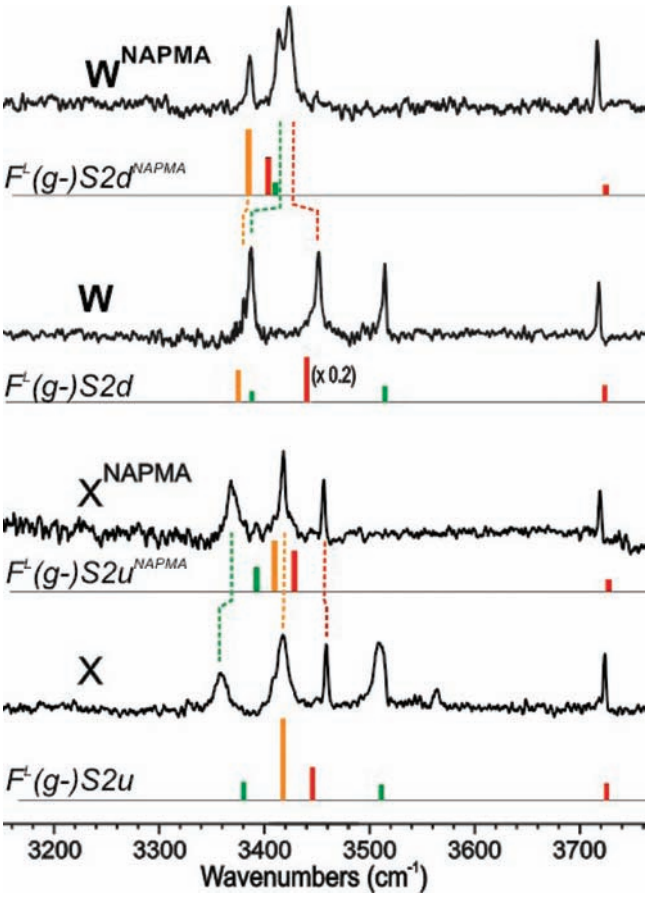

Figure 5. IR/UV double-resonance spectra of conformers **W** and **X**, compared with those of their NAPMA analogues. The calculated frequencies of the $F^L(g-)S2d$ and $F^L(g-)S2u$ conformers for both NAPA and NAPMA molecules are also presented: sticks represent the OH (red), NH1 (orange), and NH_2H_3 for NAPA or NH_2 for NAPMA (green) stretching modes (see Figure 1 for atom labels). Dotted lines highlight the correspondences that occur between **W** and **X** and their NAPMA analogues.

W. The difference between the calculated frequencies of $F^L(g-)S2d$ and the experimental frequencies of **W** is never larger than 11 cm^{-1} (Table 2). Such a good agreement is not reached for any other calculated conformations (Table 1) for which at least one frequency is off by more than 30 cm^{-1}. The expected agreement of $\pm\sim$20 cm^{-1} is then reached for only one conformation, making the assignment of **W** unambiguous. This assignment is supported by the comparison between the NAPMA analogous of $F^L(g-)S2d$ and $\mathbf{W}^{\mathbf{NAPMA}}$ (Figure 5 and SI, Figures S3 and S5).

X. Two conformers could possibly match the IR spectrum of *X* with a similar frequency agreement: $F^L(g-)S2u$ (Figure 6), together with $F^L(a)S2u$, its rotamer with an (a) orientation of the phenyl side chain instead of $(g-)$. However, $F^L(a)S2u$ has one major difference compared to $F^L(g-)S2u$ (Table 1 and SI, Figure S4): its most red-shifted band is the peptide NH stretch, which does not fit with the previously deduced assignment of this band to the NH_2^{sym} mode (section 4). One must conclude that $F^L(g-)S2u$ is the only conformer that can be assigned to *X*. This assignment is again supported by the comparison between the NAPMA analogues of $F^L(g-)S2u$ and $\mathbf{X}^{\mathbf{NAPMA}}$ (Figure 5 and SI, Figures S4 and S5). The typical frequency agreement of $\pm\sim$20 cm^{-1} is also reached, as the worst agreement is obtained for the NH_2^{sym} mode, with a 21 cm^{-1} discrepancy (Table 2).

Y. The best structure that matches conformer **Y**, $F^L(g+)S1u$ (Figure 6), is compatible with the conclusions of the Experimental Results, as it is made of a γ-turn structure with a NH$-\pi$ interaction and a water molecule in site *S1*. Actually, only four conformers are expected to fulfill these conditions: $F^L(g+)S1u$, $F^L(g+)S1d$, $F^D(g-)S1u$, and $F^D(g-)S1d$. The γ-turn is a chiral structure[18] that is L or D, and the water molecule can be a H-bond acceptor with one or the other lone pair leading to the OH free group pointing in two different directions. Both $F^D(g-)S1$ structures can be ruled out, as their NH_2^{sym} bands are predicted to be too red-shifted, at 3314 cm^{-1} (Table 1). However, it is impossible to discriminate between $F^L(g+)S1u$ and $F^L(g+)S1d$, as their calculated frequencies are virtually identical, within $\sim$3 cm^{-1}. Conformer **Y** will then refer to one structure or the other in the rest of the paper, although only one is shown in Figure 6. One can notice that the agreement here is slightly worse than that usually observed for isolated peptides ($\pm\sim$20 cm^{-1}, SI, Figure S1), as the NH_2^{sym} and OH(1) modes are predicted respectively at 29 and 23 cm^{-1} from the experimental value.

Z. Finally, only one conformer, $E(a)S3v$ (Figure 6), is fully consistent with the experimental band assignment of conformer **Z** (section 4). The NH stretch frequency is, however, poorly predicted, with a mismatch of 36 cm^{-1}. An underestimated coupling between the NH and NH_2^{sym} modes could explain why the usual $\pm\sim$20 cm^{-1} accuracy agreement is not reached. The frequency difference between these modes is going from 27 cm^{-1} for uncorrected frequencies down to only 11 cm^{-1} after applying the mode-specific scaling procedure, suggesting that a coupling may not be correctly estimated by the calculation (SI, Appendix S1). In particular, such a coupling between the NH and NH_2^{sym} modes could, for instance, explain why the NH_2^{sym} mode is observed at 3440 cm^{-1}, significantly shifted to the blue compared to conformer **A** of isolated NAPA, for which a similar $NH_2-\pi$ interaction is observed[33] at 3426 cm^{-1}. The poor frequency agreement could also suggest that B97-D does not describe accurately this conformation, where the position of the water molecule is the result of a subtle compromise between the H-bond and additional interactions with the phenyl ring (Figure 6).

6. DISCUSSION

6.1. Microsolvation Structural Effects. Conformers **W** and **X** are both $F^L(g-)S2$ conformations in which the peptide has a folded C_7^L structure with the phenyl chain in the $(g-)$ position. These conformers can then be directly compared to the $F^L(g-)$ conformer of NAPA (conformer **C**) in order to estimate the structural effects of monohydration on the peptide. Such a comparison will demonstrate how the hydration on one side of the molecule affects the whole conformation of the peptide, and in particular the intramolecular H-bond, which is on the opposite side.

Table 2 shows that the NH_2^{sym} mode is experimentally blue-shifted for both conformers **W** and **X** upon solvation. This blue-shift denotes a lengthening of the C_7 H-bond (O1$-$H2 distance in Table 2) in the hydrate, which is qualitatively well reproduced by the calculated structures with H-bonds longer by 29 and 23 pm. These elongated H-bonds can be seen as the consequence of the forces applied on atoms H1 and O2 by the bridging water in site *S2*. In order to optimize these intermolecular H-bonds, the

Table 2. Experimental (Bold) and Theoretical (Italic) Data of NAPA (Bottom) and NAPA:Water 1:1 Complex (Top) Conformers

	vibrational frequency (cm^{-1})					ΔG^{corr} (kJ mol^{-1})[a]		distance (pm)[c]	
conformer (abundance)	NH	NH_2^{sym}	NH_2^{anti}	OH(2)	BE (kJ mol^{-1})[b]	0 K	300 K	O1−H2	H1−O2
				NAPA:Water 1:1					
W (34%)	**3380**	**3388**	**3515**	**3720**					
F^L(g−)S2d	*3376*	*3389*	*3516*	*3725*	*27 (A); 30 (C)*	*2*	*4*	*232*	*319*
X (48%)	**3418**	**3360**	**3510**	**3723**					
F^L(g−)S2u	*3418*	*3381*	*3512*	*3727*	*26 (A); 29 (C)*	*2*	*3*	*226*	*325*
Y (10%)	**3439**	**3360**	**3460**	**3718**					
F^L(g+)S1u	*3442*	*3331*	*3464*	*3718*	*25 (B)*	*6*	*8*	*204*	*385*
Z (8%)	**3394**	**3440**	**3543**	**3722**					
E(a)S3v	*3430*	*3419*	*3535*	*3722*	*18 (A)*	*10*	*4*	*501*	*226*
I(a)u	*3456*	*3280*	*3503*	*3723*	*29 (A), 32 (C)*	*0*	*2*	*354*	*279*
E(a)S2d	*3305*	*3414*	*3531*	*3717*	*24 (A)*	*4*	*1*	*476*	*257*
F(a)S2d	*3343*	*3403*	*3522*	*3725*	*29 (A)*	*2*	*4*	*241*	*310*
				NAPA					
A (79%)	**3434**	**3426**	**3543**						
E(a)	*3438*	*3418*	*3534*	−	−	*0*†	*0*†	*499*	*228*
B (11%)	**3438**	**3342**	**3516**						
F^L(g+)	*3438*	*3347*	*3518*	−	−	*2*†	*5*†	*202*	*388*
C (10%)	**3466**	**3348**	**3517**						
F^L(g−)	*3466*	*3343*	*3514*	−	−	*3*†	*3*†	*203*	*374*

[a] Gibbs energies are calculated at the RI-B97-D/TZVPP level and corrected for intermolecular BSSE. The reference for these relative energies is the lowest energy conformer of the NAPA:water 1:1 complex at the temperature considered. For energies marked with †, the reference is the lowest energy conformer of NAPA (**A**). [b] The binding energies (BE) of the NAPA:water 1:1 complexes corrected for BSSE are given for several dissociation limits, corresponding to the different conformers of NAPA noted in parentheses. [c] Intramolecular distances are given in order to quantify the folded (short O1−H2 and large H1−O2 distances) or extended (large O1−H2 and short H1−O2 distances) character of the peptide conformation.

peptide backbone has to adopt a slightly new conformation, shortening the H1−O2 distance from 374 pm in conformer **C** down to 319 and 325 pm in **W** and **X**, respectively. A mechanical consequence of this adaptation of site ***S2*** upon hydration is the opening of the γ-turn: the resulting blue-shift of the NH_2^{sym} mode is then the experimental evidence of the weakening of the C_7 H-bond and the deformation of the whole peptide structure induced by the water molecule. The impact of microhydration on the γ-turn structure can also be reported on a Ramachandran map[50] (Figure 7a). Conformer **C** is described by $(\varphi,\psi) = (-85°,72°)$, which are typical values for γ-turns.[51] In contrast, **W** and **X** exhibit slightly different values, $(-85°,90°)$ and $(-84°,88°)$, respectively. It is interesting to note that the resulting microsolvation step in the Ramachandran map is clearly made in the direction of the polyproline II helix domain, typically found around angles $(-90°,135°)$, and supposed to be the most stable structure for small peptide chains in solution when solvation is completed.[4,9,52] As such a polyproline II helix does not have any intramolecular H-bond, stepwise hydration of the isolated peptide is then expected to break the C_7 H-bond. Both **W** and **X** conformations nicely illustrate how the first water molecule takes part in this process by weakening the intramolecular H-bond and justify that they can be considered as the first intermediates of the solvation process. This significant change of structure in **W** and **X** compared to the nonsolvated conformer **C** is also consistent with the UV spectrum. The UV origin transitions are indeed blueshifted respectively by 127 and 89 cm^{-1}, as opposed to smaller shifts of typically ∼10 cm^{-1} observed when solvation occurs on a rigid site and has no significant impact on the molecular conformation.[25,26]

If **W** and **X** differ mainly by the orientation of the water molecule as they are respectively assigned to ***F^L(g−)S2d*** and ***F^L(g−)S2u***, this is not the only difference in geometry, as suggested by the experimental UV and IR results. The structure of the solvation site can be monitored by the H1−O2 distance (Table 2), which is predicted 6 pm shorter in **W** as compared to **X**. This reveals a different peptide−water interaction, which also affects the secondary structure, as the C_7 H-bond is 6 pm longer in **W**. The calculated NH frequency difference of ∼40 cm^{-1} between **W** and **X** also reveals that the intermolecular distance is shorter in **W** and explains why it is possible to discriminate

dx.doi.org/10.1021/ja108643p | J. Am. Chem. Soc. 2011, 133, 3931–3942

between these conformers through their IR signatures. This is in contrast with the **Y** conformer, where $F^L(g+)S1d$ and $F^L(g+)S1u$ have very similar structures (section 5). The origin of the difference between **W** and **X** could lie in a stabilizing interaction between a H atom of the CH_2 group of the side chain and a lone pair of water in conformer **W** ($d(CH-O^{water})$ = 250 pm). In conformer **X**, this interaction is replaced by a CH_2−HO interaction, which appears to cause a slightly different geometry ($d(CH-O^{water})$ = 258 pm). All these structural differences between **W** and **X** also impact the side-chain position, eventually contributing to a relatively large separation (38 cm^{-1}) of the phenyl $\pi^* \leftarrow \pi$ transitions. In addition, the intramolecular H-bond, shortened by 6 pm when flipping water from **W** to **X**, can be directly correlated to the predicted frequency change for the NH_2^{sym} mode (−8 cm^{-1}), qualitatively supported by the experiment (−28 cm^{-1}). The quantitative mismatch, however, suggests that the impact of water orientation on the backbone geometry is underestimated by the B97-D method. It is then experimentally and theoretically suggested that the isomerization path between **W** and **X** not only is characterized by a simple flip of the water molecule but also involves backbone deformations. Tunneling isomerization usually associated with such water flipping[53] is then not expected between **W** and **X**, which is confirmed by the experimental observation of two conformers that do not interconvert within the time delay between IR and UV laser in the experiment (∼20 ns). The corresponding isomerization barrier has been calculated at ∼3 kJ mol^{-1} for the alaninamide−water complex[53] and is expected to be of the same order of magnitude between **W** and **X**. Unfortunately, the theoretical accuracy needed to investigate such a barrier is still beyond the capabilities of the B97-D method on these systems, according to the uncertainty in the structural description of the minima (discrepancies between experimental and scaled theoretical frequencies) as well as in their relative energies.

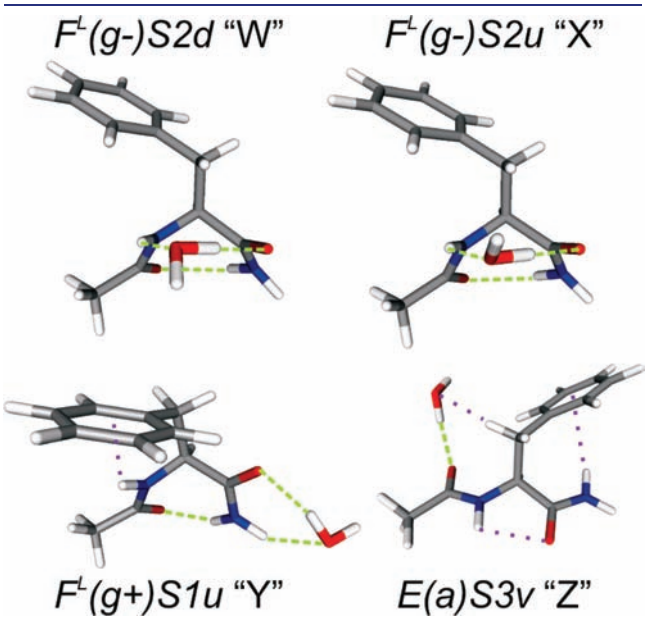

Figure 6. RI-B97-D/TZVPP minima $F^L(g-)S2d$, $F^L(g-)S2u$, $F^L(g+)S1u$, and $E(a)S3v$ assigned to conformers **W**, **X**, **Y**, and **Z**. Weak (···) and strong (---) inter- or intramolecular interactions are also shown.

Conformer **Y** is an $F^L(g+)S1$ structure where the peptide is nearly identical to conformer **B** of NAPA (Figure 7a). As the B97-D structure might not reproduce accurately the geometry of this conformer according to a slightly worse frequency agreement than for **W** and **X**, the structure analysis will be limited to

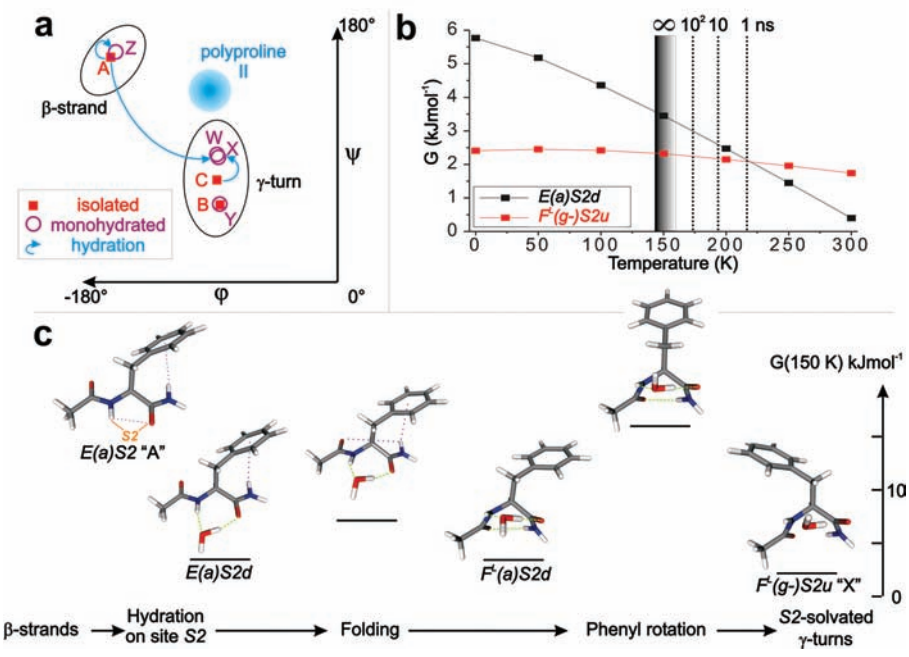

Figure 7. (a) Ramachandran map of the assigned isolated, monohydrated NAPA conformations. Typical area of β-strand, γ-turns, and polyproline II structures are also shown. Blue arrows indicate the transformations, deformation or isomerization, upon microsolvation. (b) Gibbs energies of the $E(a)S2d$ and $F^L(g-)S2u$ conformers at several temperatures. RRKM-estimated typical reaction times for the conformational isomerization of panel c are also shown. (c) Energetics of the solvation-induced isomerization of conformer **A** at 150 K estimated as being the minimum temperature needed for the reaction to occur.

dx.doi.org/10.1021/ja108643p | J. Am. Chem. Soc. 2011, 133, 3931–3942

the following considerations. Table 2 shows that the intramolecular C_7 H-bond is predicted not to be affected by the solvation, with a negligible stretch of 2 pm. Owing to the position of water in **S1**, no significant changes of the peptide structure are expected, as no conformational freedom exists to accommodate the water molecule since the O2 and H3 atoms belong to the same peptide plane. This conservation of the structure of **B** upon microsolvation is also supported by the experimental observation that the NH stretch, which is sensitive to the relative orientations of the NH1 group and the phenyl ring, has virtually the same value: 3438 (**B**) and 3439 cm^{-1} (**Y**). The small red-shift (13 cm^{-1}) of the $\pi^* \leftarrow \pi$ transitions also suggests[26] that the γ-turn in **Y** retains a structure very similar to that of **B**.

Conformer **Z**, assigned to ***E(a)S3v***, is the only extended C_5 solvated structure observed in our experiment. It can be directly compared to **A**, the main NAPA conformer observed, where the peptide has a conformation ***E(a)***. On the one hand, **A** and **Z** have identical NH_2^{anti} stretch frequencies; however, on the other hand, the NH and NH_2^{sym} modes are 40 and 14 cm^{-1} red- and blue-shifted, respectively (Table 2). These shifts could be the result of a coupling between these modes in the microsolvated peptide (section 5). The red-shift of the NH mode may also be explained by the polarization of the peptide bond by the water molecule. The 73 cm^{-1} UV shift of the origin of the $\pi^* \leftarrow \pi$ transition is also consistent with a change of the phenyl ring environment. However, the bad IR frequency agreement between experiment and theory prevent us from making a detailed structure analysis from the B97-D geometry. We have therefore no reliable evidence about how the β-strand structure is affected by the hydration on site ***S3***.

6.2. Conformational Energetics and Microhydration Dynamics in the Jet. It is clear from the calculated relative energies given in Table 1 that the observed conformational distribution extracted from our experiment is not consistent with a thermal equilibrium. As an example, according to the B97-D Gibbs energies in the 0−300 K temperature range, one would expect to observe the global minimum of the PES, conformers **I**, as being the most populated conformations (Figure 2 and Tables 1 and 2). Similarly, conformers ***F^L(g+)S1*** assigned to **Y** should not be observed due to their relatively high energy, assuming their population is controlled by thermal equilibrium conditions. A thermal equilibrium between conformations would then imply that the B97-D energetics is wrong by at least ∼10 kJ mol^{-1} and/or that the R2PI detection efficiency is highly conformer-dependent. Although these two explanations for the apparent discrepancy between experiment and theory cannot be completely ruled out, a few considerations make them both appear unlikely for this system. First, a ∼10 kJ mol^{-1} error is not expected for such a small peptide: Gibbs energies of the monomers in the 0−300 K range (Table 2) reproduce the experimentally observed distribution with a ∼2 kJ mol^{-1} accuracy. If we now examine the capability of R2PI to detect all the conformations produced in the supersonic expansion, one can notice that the proportion of 1:1 clusters detected is ∼30% of the monomer signal. This high proportion of clusters suggests that all major conformations existing in the molecular beam are detected. In addition, R2PI has proven to reliably detect conformers with a large variety of environments of the phenyl ring: (**g**+), (**g**−), and (**a**) orientations; NH−π interactions; folded or extended backbones. These considerations suggest that conformer-dependent dynamics in the excited state are not expected to strongly bias the conformational distribution for such a phenylalanine-based peptide. The origin of the discrepancies between the observed conformational distribution and the B97-D Gibbs energy is then believed to lie in the assumption of a thermal equilibrium between conformations.

If not controlled by a thermal equilibrium, the conformational distribution of the NAPA:water complexes may be controlled by the initial distribution of the isolated peptide. The aim of the next paragraph is to propose a tentative scheme for the course of events leading to the observed conformational distribution of the NAPA:water clusters.

If we consider the initial internal energy of the laser-desorbed peptide before cooling in the expansion (∼33 kJ mol^{-1} at 300 K, estimated from harmonic vibrational frequencies), a complete conformational exploration of the PES is possible. In particular, Strodel and Wales have shown,[54] on the isolated capped alanine, that the free energy barrier between the C_5 and C_7 conformers at 298 K is only ∼7 kJ mol^{-1} and that the folding/unfolding motion related to the conformational isomerization between these structures is completed within a few picoseconds, i.e., much faster than the characteristic time of our experiment (∼1 μs).[55] Cooling in the expansion then traps these conformations of NAPA, and the resulting experimental conformational distribution is consistent with thermal equilibrium conditions according to the calculated RI-B97-D/TZVPP Gibbs energies of the conformers in the 0−300 K temperature range (Table 2). In the NAPA:water system, however, such a complete exploration of the PES is not expected to occur in our experiment, as both molecules first need to be cooled before they effectively stick together and a stable complex can be formed. The fact that the most stable conformers are not observed (conformers ***I***, Table 1 and Figure 4) gives us an interesting clue on the mechanism that controls the conformational distribution. The backbone of type ***I*** (Figure 2) can be seen as a folded structure where water is inserted in the C_7 H-bond. If water were attached to NAPA when it has still enough internal energy to cross over the barrier between the extended and the folded structures, one would expect the hydrated peptide to explore the well corresponding to ***I***, eventually leading to its observation. One can then consider that, just before water finally sticks to the NAPA molecules in the expansion, the internal energy content of the peptides is already low enough that it can no longer allow their folding/unfolding isomerization. In other words, microsolvation occurs on NAPA molecules already trapped in their wells, identified as the **A**, **B**, and **C** conformers. This is fully consistent with the observation that complexes are formed within the pulsed supersonic expansion only when peptides are laser-desorbed 35 μs later than the usual optimum value to detect monomers, i.e., not until good cooling conditions are achieved in the expansion.[56] It is then legitimate to consider these results as the experimental microhydration of **A**, **B**, and **C**. The final conformational distribution of the microsolvated species is then expected to "keep the memory" of the initial distribution of the isolated species instead of being governed by a thermal equilibrium.

The three conformers of NAPA, **A**, **B**, and **C**, are now considered with their main barrierless hydration sites (Figure 8) in order to propose a microhydration scheme for this peptide:

Conformer **B** is the only conformer having only one solvation site available (***S1***), which allows the water molecule to bind with a barrierless pathway. Monohydration of **B** on site ***S1*** leads then directly to ***F^L(g+)S1***, assigned to conformer **Y**, which is thus expected to be formed in the expansion despite having higher energy than other non-observed species.

Conformer **C** has one more solvation site (***S2***) compared to **B**, and hydration of this site leads to conformers ***F^L(g−)S2d*** and

dx.doi.org/10.1021/ja108643p |*J. Am. Chem. Soc.* 2011, 133, 3931–3942

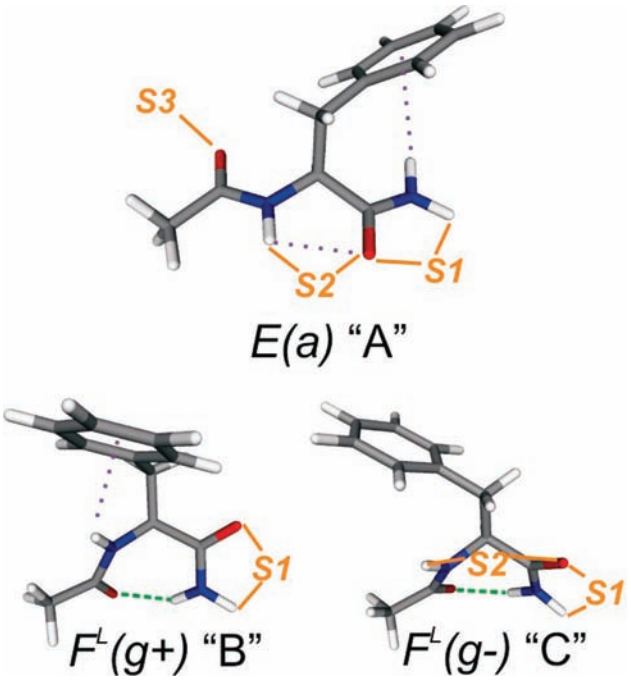

Figure 8. NAPA conformers assigned to **A**, **B**, and **C** with their hydration sites ***S1***, ***S2***, and ***S3***. These barrierless solvation sites are the only ones to enable the formation of at least one strong intermolecular H-bond, and they are considered as the main hydration sites of these conformations.

$F^L(g-)S2u$, assigned to **W** and **X**. Higher energy conformers $F^L(g-)S1d$ and $F^L(g-)S1u$ are also expected to be formed from the barrierless solvation of **C** in site ***S1***. However, these conformations are not observed, suggesting that the more stable solvation site **S2** is preferred. The additional energy brought by the intermolecular H-bond (~25 kJ mol^{-1}) when water binds in ***S1*** can indeed be used by the NAPA:water system to explore more of the PES and favor the $F^L(g-)S1 \rightarrow F^L(g-)S2$ isomerization.

Monohydration of conformer **A** appears to be even more complex, as three solvation sites are available. However, one has to notice that (i) **Z** can result from the barrierless hydration of conformer **A** on site ***S3*** and (ii) conformer **Z** is the only one that retains the peptide conformation $E(a)$ in the relaxed complexes.

At this stage, a first solvation scheme could already be proposed to account for the conformers observed in our experiment as being the result of barrierless monohydration of NAPA conformers: $\mathbf{A} + H_2O \rightarrow \mathbf{Z}$; $\mathbf{B} + H_2O \rightarrow \mathbf{Y}$; $\mathbf{C} + H_2O \rightarrow \mathbf{W/X}$. However, this solvation scheme could not fit with the relative abundances observed, as **A** accounts for almost 80% of the NAPA species in the expansion, but only ~8% of the NAPA:water complexes (**Z**) have an $E(a)$ backbone type that can be considered as the result of the direct hydration of **A**. The observed monohydrated species are indeed mainly folded, with 82% of the population (**W** + **X**) having an $F^L(g-)S2$ structure. It is then suggested, on the basis of the observed conformational distribution, that a solvation-induced population transfer exists between the isolated $E(a)$ conformation (**A**) and the $F^L(g-)S2$ monohydrated peptides (**W**/**X**). In addition, the conformers resulting from the barrierless solvation of **A** in sites ***S1*** or ***S2*** are surprisingly not observed, despite these sites being apparently better binding sites than ***S3***, according to their relative energies (Table 1). These non-observed conformers, $E(a)S1$ and $E(a)S2$, lead us to consider that their isomerization may be responsible for the above-mentioned solvation-induced population transfer. In this respect, the path $\mathbf{A} + H_2O(S2) \rightarrow E(a)S2 \rightarrow F^L(a)S2 \rightarrow F^L(g-)S2$ was investigated theoretically in order to estimate if such a population transfer is supported by B97-D calculations. Gibbs energies of $E(a)S2$ and $F^L(g-)S2$ at several temperatures are presented in Figure 7b. Transition states have also been calculated and are displayed in Figure 7c. The highest barrier of the path (14 kJ mol^{-1}) corresponds to the phenyl rotation $F^L(a)S2 \rightarrow F^L(g-)S2$, and it can be estimated from the vibrational energy that this barrier cannot be overcome if the temperature of the NAPA:water complex is lower than ~150 K. RRKM theory[57] has also been used to roughly estimate the isomerization rate at several temperatures (Figure 7b): it shows that, above about 170 K, isomerization is likely to occur within the time scale of our experiment (>100 ns). As a facile redistribution of the binding energy can be anticipated in such flexible systems,[30] it can be postulated that the conversion of this energy in $E(a)S2$ immediately after its formation in the expansion (24 kJ mol^{-1}, Table 2) leads to an initial vibrational temperature of the complex that is estimated from harmonic frequencies to be at least ~220 K, which would be enough to trigger isomerization. In conclusion, the isomerization $E(a)S2 \rightarrow F^L(g-)S2$ is likely to take place efficiently while the complex is formed and cooled during the supersonic expansion. A solvation-induced population transfer between **A** and **W**/**X** is then in agreement with B97-D calculations, making a solvation-induced isomerization $\mathbf{A} + H_2O(S2/S1) \rightarrow E(a)S2 \rightarrow \mathbf{W/X}$ the best explanation for the NAPA:water relative abundances observed and for the experimental non-observation of the $E(a)S2$ and $E(a)S1$ conformations.

To conclude this section, a conformer-dependent and site-dependent microhydration scheme is proposed to account for the IR spectroscopy and the relative abundances observed on the UV spectrum:

$$\mathbf{A} + H_2O(S2/S1) \rightarrow E(a)S2 \rightarrow \mathbf{W/X}; \quad \mathbf{A} + H_2O(S3) \rightarrow \mathbf{Z}$$

$$\mathbf{B} + H_2O(S1) \rightarrow \mathbf{Y}$$

$$\mathbf{C} + H_2O(S2/S1) \rightarrow \mathbf{W/X}$$

This scheme also implies that the complex is trapped in the well of conformer **Z** when water approaches the NAPA molecule from the ***S3*** side: isomerizations toward lower energy conformations like **W**/**X** or **I** presumably involve high-energy transition states that keep the system in the **Z** basin. If we consider, for instance, the path $\mathbf{Z} \rightarrow E(a)S2 \rightarrow \mathbf{W/X}$, the first step is very similar to the water shuttling between the solvation sites of the *trans*-formanilide, which has been measured[21] to cost ~10−12 kJ mol^{-1}. As this path $\mathbf{Z} \rightarrow E(a)S2$ would siphon off the population **Z**, this shuttling barrier in NAPA:water is then expected to be high enough to enable the detection of **Z**. The ~18 kJ mol^{-1} internal energy available after water binding in site ***S3*** (binding energy of **Z**, Table 2) might thus be not enough to efficiently trigger this isomerization during the expansion.

7. CONCLUSION

A combined experimental and theoretical study of the monohydration of a model peptide chain in the gas phase has revealed a conformer-dependent and site-dependent microhydration scheme, illustrating the flexibility of the backbone peptide and its sensitivity to its environment.

The NAPA:water system interestingly exhibits three kinds of solvation of the capped phenylalanine, depending on the modification of the secondary structure induced by the water molecule (Figure 7a): (a) Hydration does not significantly change the structure of the peptide conformer, like in the $\mathbf{B} + H_2O(\boldsymbol{S1}) \rightarrow \mathbf{Y}$ solvation. (b) Hydration induces distortions of the secondary structure, but the solvated conformer can still be identified. This is the case for the solvation of **C**, $\mathbf{C} + H_2O(\boldsymbol{S2/S1}) \rightarrow \mathbf{W/X}$, which distorts the γ-turn structure toward the polyproline II helix structure. (c) Finally, monohydration can induce a conformational isomerization like the folding of β-strand into γ-turn structures experimentally observed and likely resulting from the $\mathbf{A} + H_2O(\boldsymbol{S2/S1}) \rightarrow \boldsymbol{E(a)S2} \rightarrow \mathbf{W/X}$ folding process. This path, supported by both B97-D calculations and experimental observations, highlights the role played by a single water molecule in peptide folding, where the hydration of the extended peptide chain **A** on site ***S2*** is accompanied by backbone deformations, which eventually leads to a complete folding and the formation of an intramolecular H-bond.

The complete hydration scheme in the supersonic expansion leads to conformational relative abundances that are not governed by a thermodynamic equilibrium but "keep the memory" of the initial conformational distribution of the isolated peptide. Some regions of the PES are not explored, which explains why conformers ***I***, predicted as the global minima of the PES, are not observed. It is possible, instead, to detect **Y** despite its high relative energy, whereas this conformer would not be observed in the case of a thermal equilibrium between conformations. These results suggest that the initial distribution of monomers in the jet is a crucial parameter for the hydrate distribution. In addition, the phenyl side chain could sterically control the accessibility of a few hydration sites on the peptide backbone. In this perspective, the investigation of the singly hydrated alanine-based peptide, accessible through microwave absorption spectroscopy,[24,58] would be of great interest. In particular, it could provide a way to observe and characterize alternative monohydrate conformations, including type ***I*** structures, which have already been observed in matrices for such an alanine-based peptide.[7]

This paper also illustrates the strength of IR/UV spectroscopy when combined to a vibrational modeling that accounts for anharmonicity. It enables us to identify and measure the conformational populations and opens up the route to barrier height measurements[59] and related experiments, such as the measurements of the binding energy of water to NAPA and its dependence upon the solvation site. This type of experiments, combined with free energy calculations using metadynamics[60] methodology, will enable spectroscopists to go beyond simple structural characterization and to document the influence of solvation upon the dynamical properties of the flexible peptide chain. Further investigations of larger hydrates would provide experimental evidence of the hydration steps followed by this system on the Ramachandran map one molecule at a time. As theory suggests that four water molecules stabilize the polyproline II structure of such a model peptide chain,[9] characterization of this structure typical of the condensed phase can be expected for a neutral cluster in the future.

■ ASSOCIATED CONTENT

Supporting Information. Scaling procedure of the calculated harmonic frequencies for comparison with the experimental spectra; experimental and theoretical results obtained on the 1:1 NAPMA:water clusters and compared to NAPA; coordinates of the main conformations discussed in the paper; and complete ref 38. This material is available free of charge via the Internet at http://pubs.acs.org.

■ AUTHOR INFORMATION

Corresponding Author
eric.gloaguen@cea.fr

■ ACKNOWLEDGMENT

Support from the French National Research Agency (ANR) is acknowledged (Grant ANR-08-BLAN-0158-01). The authors thank Dr. Richard Plowright for improving the quality of this manuscript.

■ REFERENCES

(1) Gaigeot, M. P. *J. Phys. Chem. B* **2009**, *113*, 10059.
(2) Kwac, K.; Lee, K. K.; Han, J. B.; Oh, K. I.; Cho, M. *J. Chem. Phys.* **2008**, *128*, 13.
(3) Maekawa, H.; Formaggio, F.; Toniolo, C.; Ge, N. H. *J. Am. Chem. Soc.* **2008**, *130*, 6556.
(4) Poon, C. D.; Samulski, E. T.; Weise, C. F.; Weisshaar, J. C. *J. Am. Chem. Soc.* **2000**, *122*, 5642.
(5) Deng, Z.; Polavarapu, P. L.; Ford, S. J.; Hecht, L.; Barron, L. D.; Ewig, C. S.; Jalkanen, K. *J. Phys. Chem.* **1996**, *100*, 2025.
(6) Roberts, G. M.; Lee, O.; Calienni, J.; Diem, M. *J. Am. Chem. Soc.* **1988**, *110*, 1749.
(7) Tarczay, G.; Gòbi, S.; Vass, E.; Magyarfalvi, G. *Vibr. Spectrosc.* **2009**, *50*, 21.
(8) Jalkanen, K. J.; Elstner, M.; Suhai, S. *J. Mol. Struct.* **2004**, *675*, 61.
(9) Han, W. G.; Jalkanen, K. J.; Elstner, M.; Suhai, S. *J. Phys. Chem. B* **1998**, *102*, 2587.
(10) Pribble, R. N.; Zwier, T. S. *Science* **1994**, *265*, 75.
(11) Zwier, T. S. *J. Phys. Chem. A* **2006**, *110*, 4133.
(12) Simons, J. P. *Mol. Phys.* **2009**, *107*, 2435.
(13) Chin, W.; Piuzzi, F.; Dimicoli, I.; Mons, M. *Phys. Chem. Chem. Phys.* **2006**, *8*, 1033.
(14) Fricke, H.; Schäfer, G.; Schrader, T.; Gerhards, M. *Phys. Chem. Chem. Phys.* **2007**, *9*, 4592.
(15) Valdes, H.; Spiwok, V.; Řezáč, J.; Řeha, D.; Abo-Riziq, A. G.; de Vries, M. S.; Hobza, P. *Chem.—Eur. J.* **2008**, *14*, 4886.
(16) Gloaguen, E.; Valdes, H.; Pagliarulo, F.; Pollet, R.; Tardivel, B.; Hobza, P.; Piuzzi, F.; Mons, M. *J. Phys. Chem. A* **2010**, *114*, 2973.
(17) Chin, W.; Piuzzi, F.; Dognon, J.-P.; Dimicoli, I.; Mons, M. *J. Chem. Phys.* **2005**, *123*, 084301.
(18) Gloaguen, E.; Pagliarulo, F.; Brenner, V.; Chin, W.; Piuzzi, F.; Tardivel, B.; Mons, M. *Phys. Chem. Chem. Phys.* **2007**, *9*, 4491.
(19) Carney, J. R.; Dian, B. C.; Florio, G. M.; Zwier, T. S. *J. Am. Chem. Soc.* **2001**, *123*, 5596.
(20) Schmitt, M.; Böhm, M.; Ratzer, C.; Vu, C.; Kalkman, L.; Meerts, W. L. *J. Am. Chem. Soc.* **2005**, *127*, 10356.
(21) Clarkson, J. R.; Baquero, E.; Shubert, V. A.; Myshakin, E. M.; Jordan, K. D.; Zwier, T. S. *Science* **2005**, *307*, 1443.
(22) Bouteiller, Y.; Gillet, J. C.; Grégoire, G.; Schermann, J. P. *J. Phys. Chem. A* **2008**, *112*, 11656.
(23) Alonso, J. L.; Cocinero, E. J.; Lesarri, A.; Sanz, M. E.; López, J. C. *Angew. Chem., Int. Ed.* **2006**, *45*, 3471.
(24) Lavrich, R. J.; Plusquellic, D. F.; Suenram, R. D.; Fraser, G. T.; Walker, A. R. H.; Tubergen, M. J. *J. Chem. Phys.* **2003**, *118*, 1253.
(25) Lee, K. T.; Sung, J.; Lee, K. J.; Kim, S. K.; Park, Y. D. *J. Chem. Phys.* **2002**, *116*, 8251.
(26) Ebata, T.; Hashimoto, T.; Ito, T.; Inokuchi, Y.; Altunsu, F.; Brutschy, B.; Tarakeshwar, P. *Phys. Chem. Chem. Phys.* **2006**, *8*, 4783.
(27) Zhu, H.; Blom, M.; Compagnon, I.; Rijs, A. M.; Roy, S.; von Helden, G.; Schmidt, B. *Phys. Chem. Chem. Phys.* **2010**, *12*, 3415.

(28) Fricke, H.; Schwing, K.; Gerlach, A.; Unterberg, C.; Gerhards, M. *Phys. Chem. Chem. Phys.* **2010**, *12*, 3511.
(29) Peteanu, L. A.; Levy, D. H. *J. Phys. Chem.* **1988**, *92*, 6554.
(30) Clarkson, J. R.; Herbert, J. M.; Zwier, T. S. *J. Chem. Phys.* **2007**, *126*, 15.
(31) Florio, G. M.; Zwier, T. S. *J. Phys. Chem. A* **2003**, *107*, 974.
(32) Çarçabal, P.; Jockusch, R. A.; Hünig, I.; Snoek, L. C.; Kroemer, R. T.; Davis, B. G.; Gamblin, D. P.; Compagnon, I.; Oomens, J.; Simons, J. P. *J. Am. Chem. Soc.* **2005**, *127*, 11414.
(33) Chin, W.; Mons, M.; Dognon, J.-P.; Piuzzi, F.; Tardivel, B.; Dimicoli, I. *Phys. Chem. Chem. Phys.* **2004**, *6*, 2700.
(34) Gerhards, M.; Unterberg, C. *Phys. Chem. Chem. Phys.* **2002**, *4*, 1760.
(35) Gerhards, M.; Unterberg, C.; Gerlach, A.; Jansen, A. *Phys. Chem. Chem. Phys.* **2004**, *6*, 2682.
(36) Piuzzi, F.; Dimicoli, I.; Mons, M.; Tardivel, B.; Zhao, Q. *Chem. Phys. Lett.* **2000**, *320*, 282.
(37) Zwier, T. S. *J. Phys. Chem. A* **2001**, *105*, 8827.
(38) Case, D.A.; et al. *AMBER 9*; University of California: San Francisco, 2006.
(39) MacKerell, A. D.; Banavali, N.; Foloppe, N. *Biopolymers* **2000**, *56*, 257.
(40) *HyperChem Professional 7.51*; Hypercube, Inc.: Gainesville, FL, 2002.
(41) Grimme, S. *J. Comput. Chem.* **2006**, *27*, 1787.
(42) Grimme, S. *J. Comput. Chem.* **2004**, *25*, 1463.
(43) Ahlrichs, R.; Bär, M.; Häser, M.; Horn, H.; Kölmel, C. *Chem. Phys. Lett.* **1989**, *162*, 165.
(44) Vázquez-Mayagoitia, A.; Sherrill, C. D.; Aprà, E.; Sumpter, B. G. *J. Chem. Theory Comput.* **2010**, *6*, 727.
(45) Bouteiller, Y.; Poully, J. C.; Desfrançois, C.; Grégoire, G. *J. Phys. Chem. A* **2009**, *113*, 6301.
(46) Graham, R. J.; Kroemer, R. T.; Mons, M.; Robertson, E. G.; Snoek, L. C.; Simons, J. P. *J. Phys. Chem. A* **1999**, *103*, 9706.
(47) Robertson, E. G.; Hockridge, M. R.; Jelfs, P. D.; Simons, J. P. *Phys. Chem. Chem. Phys.* **2001**, *3*, 786.
(48) Matsuda, Y.; Ebata, T.; Mikami, N. *J. Chem. Phys.* **1999**, *110*, 8397.
(49) Florio, G. M.; Gruenloh, C. J.; Quimpo, R. C.; Zwier, T. S. *J. Chem. Phys.* **2000**, *113*, 11143.
(50) Richardson, J. S. *Adv. Protein Chem.* **1981**, *34*, 167.
(51) Smith, J. A.; Pease, L. G. *Crit. Rev. Biochem.* **1980**, *8*, 315.
(52) Shi, Z. S.; Olson, C. A.; Rose, G. D.; Baldwin, R. L.; Kallenbach, N. R. *Proc. Natl. Acad. Sci. U.S.A.* **2002**, *99*, 9190.
(53) Lavrich, R. J.; Tubergen, M. J. *J. Am. Chem. Soc.* **2000**, *122*, 2938.
(54) Strodel, B.; Wales, D. J. *Chem. Phys. Lett.* **2008**, *466*, 105.
(55) Miller, D. R. . In *Atomic and Molecular Beam Methods*; Scoles, G., Ed.; Oxford Univeristy Press: Oxford, 1988; p 14.
(56) Li, S. J.; Bernstein, E. R. *J. Chem. Phys.* **1992**, *97*, 792.
(57) Baer, T.; Hase, W. L. *Unimolecular Reaction Dynamics: Theory and Experiments*; Oxford University Press: New York, 1996.
(58) Aviles-Moreno, J. R.; Demaison, J.; Huet, T. R. *J. Am. Chem. Soc.* **2006**, *128*, 10467.
(59) Dian, B. C.; Clarkson, J. R.; Zwier, T. S. *Science* **2004**, *303*, 1169.
(60) Laio, A.; Parrinello, M. *Proc. Natl. Acad. Sci. U.S.A.* **2002**, *99*, 12562.